Acta Mech 218, 115–132 (2011)
DOI 10.1007/s00707-010-0404-8

J. T. Chen · K. H. Chou · Y. T. Lee

A novel method for solving the displacement and stress fields of an infinite domain with circular holes and/or inclusions subject to a screw dislocation

Received: 19 November 2009 / Revised: 8 June 2010 / Published online: 17 November 2010
© Springer-Verlag 2010

Abstract In this paper, the degenerate kernel and superposition technique are employed to solve the screw dislocation problems with circular holes or inclusions. The problem is decomposed into the screw dislocation problem with several holes and the interior Laplace problems for several circular inclusions. Following the success of the null-field integral equation approach, the typical boundary value problems can be solved easily. The kernel functions and unknown boundary densities are expanded by using the degenerate kernel and Fourier series, respectively. To the authors' best knowledge, the angle-type fundamental solution is first derived in terms of degenerate kernel in this paper. Finally, four examples are demonstrated to verify the validity of the present approach.

1 Introduction

The subject of dislocation is essential for understanding various physical and mechanical properties of crystalline solids. Many researchers investigated dislocation problems in the past years. Smith [18] successfully solved the problem of the interaction between a screw dislocation and a circular or elliptic inclusion contained within an infinite body by using the complex-variable function and circle theorem. Besides, uniform anti-plane remote shear was also considered at the same time. Dislocation problems have been solved by using the complex variable method [1,3]. Dundurs [9] solved the screw dislocation with circular inclusion problem by using the image technique. Later, Sendeckyj [17] employed the complex-variable function in conjunction with the inverse point method to solve the problem of the screw dislocation near an arbitrary number of circular inclusions. Honein et al. [13] extended the circle theorem to solve the problem of an elastic body containing an elastic circular inclusion and subject to arbitrary loading. Sudak [19] and Jin and Fang [14] solved the problem of the screw dislocation interacting with an imperfect interface by using the complex-variable technique. Such a problem was also solved by using the image technique and Fourier transform by Fan and Wang [10]. Later, Fang and Liu [11] extended the complex-variable function and Riemann-Schwarz's symmetry principle to solve the problem of the interaction of a screw dislocation with a circular nano-inhomogeneity incorporating interface stress. Almost all the above problems were solved by using the complex-variable technique. Its extension to three-dimensional cases may be limited. A more general approach is nontrivial for further investigation.

In this paper, we introduce the degenerate (or so-called separable) kernel for the angle-type fundamental solution (θ) instead of radial-basis one ($\ln r$) to represent the screw dislocation solution. The terminology of the degenerate kernel is not coined by the authors, but refers to [2,12,16]. The degenerate kernel is also

J. T. Chen · K. H. Chou · Y. T. Lee
Department of Harbor and River Engineering, National Taiwan Ocean University, Keelung, Taiwan

J. T. Chen (✉)
Department of Mechanical and Mechatronics Engineering, National Taiwan Ocean University, Keelung, Taiwan
E-mail: jtchen@mail.ntou.edu.tw

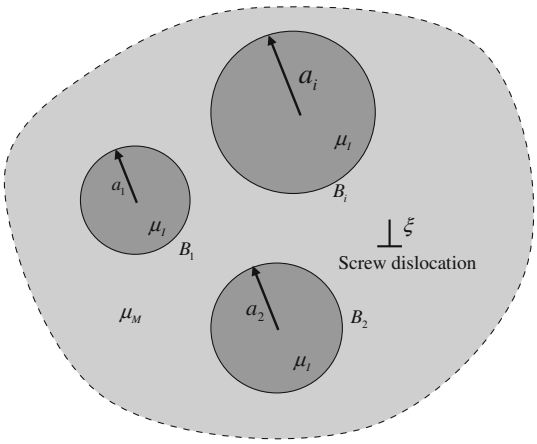

Fig. 1 An infinite-plane problem with arbitrary number of circular inclusions subject to the screw dislocation

defined in the revised manuscript by $K(x,s) = \sum_{j=1}^{\infty} A_j(s)B_j(s)$. To our best knowledge, the degenerate kernel for angle-type fundamental solution was not found in the literature. The proposed approach leads to real (as opposed to complex) equations that are free of singular integrals even when collocated on the boundary of a domain. A screw dislocation solution is decomposed into two parts. One is the screw dislocation problem with several holes, and the other is the interior Laplace problems for several circular inclusions. The interior problems can be solved by using the null-field integral approach [6]. After superimposing the two solutions, the governing equation and boundary conditions can be satisfied automatically. The present approach offers a few attractive features. First, the integrals in the boundary integral equation method (BIEM) are made simple by avoiding the senses of Cauchy and Hadamard principal values. Second, the extension of this idea to a three-dimensional problem may be straightforward. Besides, the proposed method can be seen as a kind of meshless method since no boundary element discretization is required. Finally, several illustrative examples are demonstrated to validate the present method.

2 Problem statements and mathematical formulation

The physical problem to be considered is shown in Fig. 1, where circular inclusions are imbedded in an infinite plane. For the anti-plane problem, we only consider the anti-plane displacement w such that

$$u = v = 0, \quad w = w(x, y), \tag{1}$$

where u and v are the vanishing components of displacement. The governing equation for the anti-plane displacement, w, in the anti-plane elasticity in the absence of body force is simplified to

$$\nabla^2 w(x, y) = 0, \quad (x, y) \in D, \tag{2}$$

where ∇^2 is the two-dimensional Laplacian operator and D denotes the domain of the interest. Therefore, the screw dislocation can be described as

$$\lim_{y \to 0} [w(x, -y) - w(x, y)] = b, \quad x \geq \xi, \tag{3}$$

where b denotes the Burgers' vector and ξ denotes the location of the screw dislocation. By taking free body along the interface between the matrix and inclusions, the problem is decomposed into two systems. One is an infinite plane with H randomly distributed circular holes subject to a screw dislocation as shown in Fig. 2a. The other is H randomly distributed circular inclusions bounded by contours B_i $(i = 1, 2, \ldots, H)$ which satisfies the Laplace equation as shown in Fig. 2b. For the problem in Fig. 2a, it can be superimposed by two parts again. One is an infinite plane subject to a screw dislocation and the other is an infinite plane with H randomly distributed circular holes, which satisfies the specified boundary conditions as shown in Fig. 2c and d, respectively. The displacement arising from the screw dislocation on each boundary in Fig. 2c by using the degenerate kernel is introduced in the next section. In order to solve the interior and exterior typical boundary

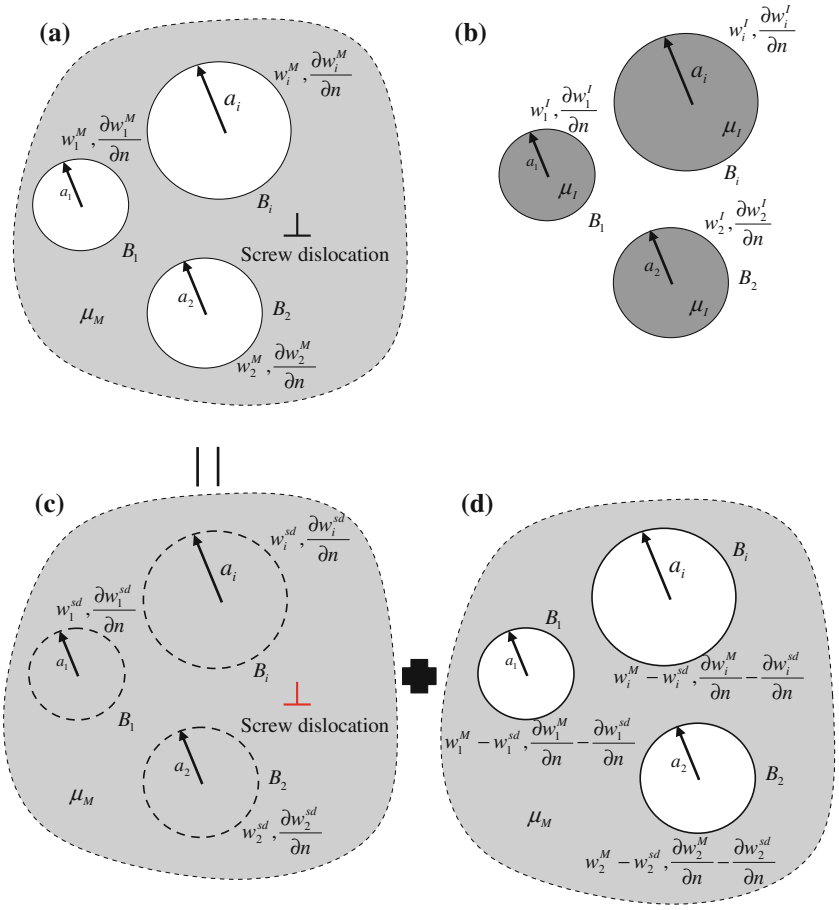

Fig. 2 **a** An infinite matrix with circular holes subject to a screw dislocation; **b** An interior Laplace problems for each circular inclusion; **c** An infinite matrix subject to a screw dislocation; **d** Exterior Laplace problems for the matrix

value problems (BVPs) in Fig. 2b and d, respectively, the null-field boundary integral formulation is reviewed and elaborated on later. According to the continuity condition on the interface, we have

$$w_i^M = w_i^I, \quad i = 1, 2, 3, \ldots, H, \tag{4}$$

$$\mu_M \frac{\partial w_i^M}{\partial n} = -\mu_I \frac{\partial w_i^I}{\partial n}, \quad i = 1, 2, 3, \ldots, H, \tag{5}$$

where μ_I and μ_M denote the shear moduli for the inclusion and matrix, respectively.

2.1 Translating the screw dislocation with respect to the center of circular boundary by using the degenerate kernel

In order to translate the screw dislocation with respect to the center of each circular boundary, the degenerate kernel is used here. The kernel function in the polar coordinate is utilized to replace the Cartesian coordinate. Therefore, the location of the screw dislocation and collocation points are expressed as $(R,\ \theta)$ and $(\rho,\ \phi)$, respectively, in polar coordinates. The position vector of the screw dislocation point is $z_s = Re^{i\theta}$. Similarly, the collocation point can be expressed by $z_x = \rho e^{i\phi}$ as shown in Fig. 3. In order to derive the degenerate kernel of screw dislocation of Laplace equation, we have

$$\ln(z_x - z_s) = \ln(re^{i\varphi}) = \ln r + i\varphi. \tag{6}$$

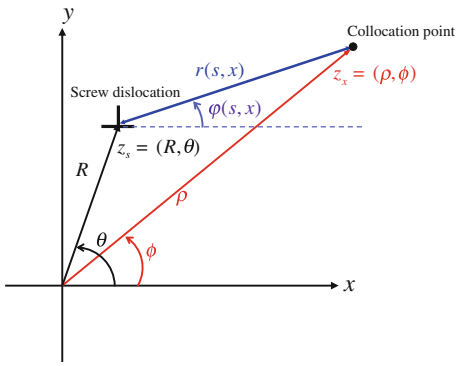

Fig. 3 Sketch for a screw dislocation

For the exterior case ($R < \rho$), Eq. (6) can be expanded as follows:

$$\begin{aligned}\ln(z_x - z_s) &= \ln(z_x) + \ln\left(1 - \frac{z_s}{z_x}\right)\\ &= \ln(\rho e^{i\phi}) - \sum_{m=1}^{\infty} \frac{1}{m}\left(\frac{z_s}{z_x}\right)^m\\ &= \ln\rho + i\phi - \sum_{m=1}^{\infty} \frac{1}{m}\left(\frac{Re^{i\theta}}{\rho e^{i\phi}}\right)^m\\ &= \ln\rho + i\phi - \sum_{m=1}^{\infty} \frac{1}{m}\left(\frac{R}{\rho}\right)^m [\cos m(\theta-\phi) + i\sin m(\theta-\phi)].\end{aligned} \tag{7}$$

Thus, the degenerate (separable) form for the fundamental solution of the screw dislocation, $\varphi(s, x)$, is obtained

$$\varphi(s, x) = \phi - \sum_{m=1}^{\infty} \frac{1}{m}\left(\frac{R}{\rho}\right)^m \sin m(\theta - \phi), \quad R < \rho. \tag{8}$$

Similarly, we also obtain

$$\varphi(s, x) = \theta + \pi + \sum_{m=1}^{\infty} \frac{1}{m}\left(\frac{\rho}{R}\right)^m \sin m(\theta - \phi), \quad R > \rho. \tag{9}$$

for the interior case ($R > \rho$). In Fig. 3, the principal angle for $\varphi(s, x)$ is defined in the interval of 0 and 2π. In order to match the physical meaning and mathematical requirement, we modify the range of interest to be between $-\pi$ and π. Thus, the fundamental solution of the screw dislocation is expressed by

$$\varphi(s, x) = \begin{cases} \varphi^I(\rho, \phi; R, \theta) = \theta + \sum\limits_{m=1}^{\infty} \frac{1}{m}\left(\frac{\rho}{R}\right)^m \sin m(\theta - \phi), & R > \rho,\\ \varphi^E(\rho, \phi; R, \theta) = \phi - \pi - \sum\limits_{m=1}^{\infty} \frac{1}{m}\left(\frac{R}{\rho}\right)^m \sin m(\theta - \phi), & R < \rho, \end{cases} \tag{10}$$

where the superscripts "I" and "E" denote the interior and exterior cases, respectively. The interior case means the collocation point in the blue region of Fig. 5 and the exterior case means the collocation point in the red region of Fig. 5, where the source is on the circular boundary. It is noted that the denominator for the degenerate kernel in Eq. (10) involves the larger argument such that the ratio test can prove the series convergence. According to the ratio test in the Calculus,

$$\lim_{m\to\infty} \left| \frac{\frac{1}{m+1}\left(\frac{\rho}{R}\right)^{m+1} e^{i(m+1)(\theta-\phi)}}{\frac{1}{m}\left(\frac{\rho}{R}\right)^{m} e^{im(\theta-\phi)}} \right| = \frac{\rho}{R} < 1, \tag{11}$$

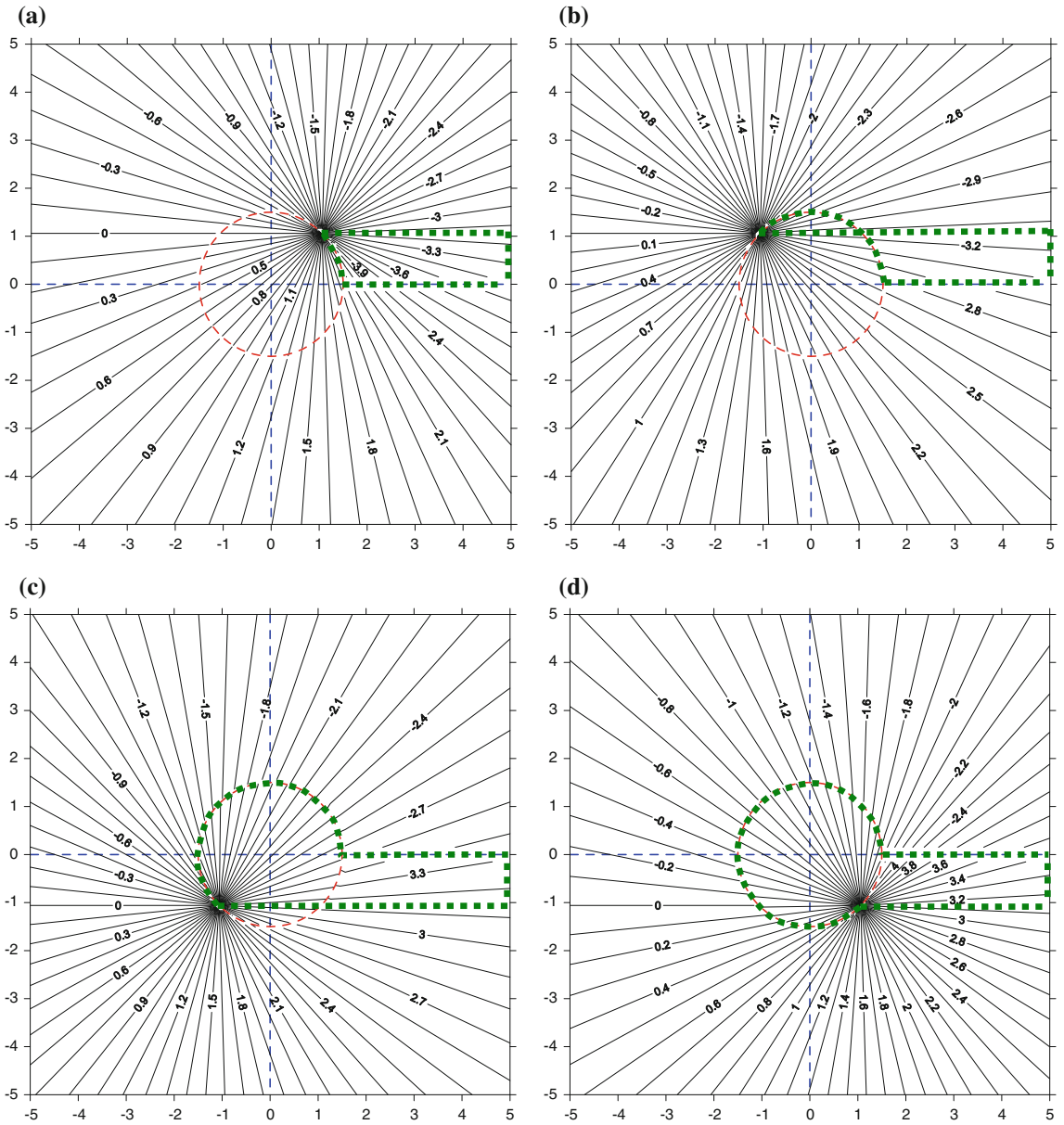

Fig. 4 **a** A screw dislocation in the first quadrant without the constraint ($R = 1.5, \theta = \pi/4$); **b** A screw dislocation in the second quadrant without the constraint ($R = 1.5, \theta = 3\pi/4$); **c** A screw dislocation in the third quadrant without the constraint ($R = 1.5, \theta = 5\pi/4$); **d** A screw dislocation in the forth quadrant without the constraint ($R = 1.5, \theta = 7\pi/4$)

the series in Eq. (7) converges, since the large argument is in the denominator of the corresponding degenerate kernel. Besides, the displacement is obtained by integrating the kernel in companion with the boundary density along the boundary. The convergence behavior can be improved after integration. In real calculation, we have $\rho \to R^+$or $\rho \to R^-$ instead of $\rho = R$ to make $z = 1$. The contour plots for the screw dislocation located at the four quadrants are shown in Fig. 4a–d, respectively. As shown in Fig. 4a–d, there are certain areas bounded by the green line where the displacement falls outside the range between $-\pi$ and π. It must be interpreted by using the principal values. We subtract 2π when the value of the potential is greater than π in order to ensure the value in the range. Similarly, we add 2π when the value is smaller than $-\pi$. It is found that all the response of screw dislocation fall into the range of definition as shown in Fig. 5. To the authors' best knowledge, the degenerate kernel for the angle-type fundamental solution was not found in the literature. Then, the displacement on each circular boundary arisen from the screw dislocation in Fig. 2c can be obtained easily by using the degenerate kernel.

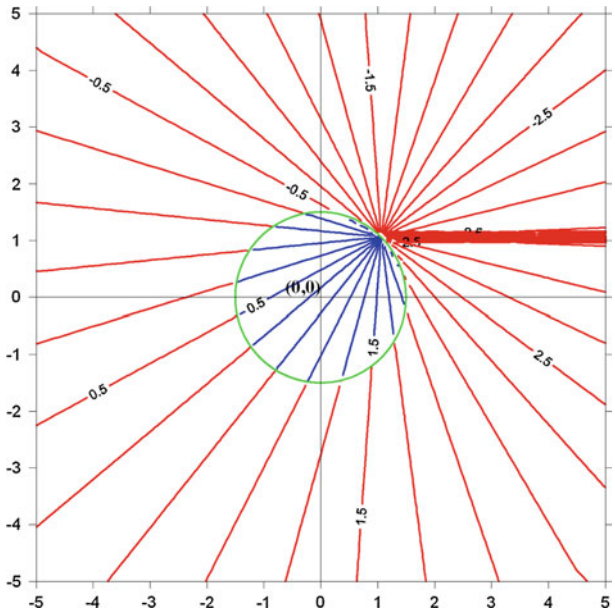

Fig. 5 A screw dislocation in the first quadrant under the constraint ($R = 1.5, \theta = \pi/4$)

2.2 Review of the null-field integral equations for typical BVPs

Following the success of null-field integral equation for interior (Fig. 2b) and exterior (Fig. 2d) BVPs, a detailed formulation is reviewed here.

2.2.1 Dual null-field integral formulation: the conventional version

Based on the dual boundary integral formulation [1] for the domain point, we have

$$2\pi w(x) = \int_B T(s,x)w(s)\mathrm{d}B(s) - \int_B U(s,x)\frac{\partial w(s)}{\partial n_s}\mathrm{d}B(s), \quad x \in D, \tag{12}$$

$$2\pi \frac{\partial w(x)}{\partial n_x} = \int_B M(s,x)w(s)\mathrm{d}B(s) - \int_B L(s,x)\frac{\partial w(s)}{\partial n_s}\mathrm{d}B(s), \quad x \in D, \tag{13}$$

where s and x are the source and field points, respectively; B is the boundary, n_x and n_s denote the outward normal vector at field point and source point, respectively; and the kernel function $U(s,x)$ is the fundamental solution, which satisfies

$$\nabla^2 U(s,x) = \delta(x-s). \tag{14}$$

The other kernel functions can be obtained as

$$T(s,x) = \frac{\partial U(s,x)}{\partial n_s}, \tag{15}$$

$$L(s,x) = \frac{\partial U(s,x)}{\partial n_x}, \tag{16}$$

$$M(s,x) = \frac{\partial^2 U(s,x)}{\partial n_s \partial n_x}. \tag{17}$$

By moving the field point x to the boundary, the dual boundary integral equations for the boundary point can be obtained as follows:

$$\pi w(x) = C.P.V. \int_B T(s,x)w(s)\mathrm{d}B(s) - R.P.V. \int_B U(s,x)\frac{\partial w(s)}{\partial n_s}\mathrm{d}B(s), \quad x \in B, \tag{18}$$

$$\pi \frac{\partial w(x)}{\partial n_x} = H.P.V. \int_B M(s,x)w(s)\mathrm{d}B(s) - C.P.V. \int_B L(s,x)\frac{\partial w(s)}{\partial n_s}\mathrm{d}B(s), \quad x \in B, \tag{19}$$

where $R.P.V.$ is the Riemann principal value, $C.P.V.$ is the Cauchy principal value and $H.P.V.$ is the Hadamard (or called Mangler) principal value. By moving the field point to the complementary domain, the dual null-field integral equations are shown below:

$$0 = \int_B T(s,x)w(s)\mathrm{d}B(s) - \int_B U(s,x)\frac{\partial w(s)}{\partial n_s}\mathrm{d}B(s), \quad x \in D^c, \tag{20}$$

$$0 = \int_B M(s,x)w(s)\mathrm{d}B(s) - \int_B L(s,x)\frac{\partial w(s)}{\partial n_s}\mathrm{d}B(s), \quad x \in D^c, \tag{21}$$

where D^c denotes the complementary domain.

2.2.2 Dual null-field integral formulation: the present version

By introducing the degenerate kernels, the collocation point can be located on the real boundary free of facing singularity. Therefore, the representations of integral equations including the boundary point can be written as

$$2\pi w(x) = \int_B T^E(s,x)w(s)\mathrm{d}B(s) - \int_B U^E(s,x)\frac{\partial w(s)}{\partial n_s}\mathrm{d}B(s), \quad x \in D \cup B, \tag{22}$$

$$2\pi \frac{\partial w(x)}{\partial n_x} = \int_B M^E(s,x)w(s)\mathrm{d}B(s) - \int_B L^E(s,x)\frac{\partial w(s)}{\partial n_s}\mathrm{d}B(s), \quad x \in D \cup B, \tag{23}$$

and

$$0 = \int_B T^I(s,x)w(s)\mathrm{d}B(s) - \int_B U^I(s,x)\frac{\partial w(s)}{\partial n_s}\mathrm{d}B(s), \quad x \in D^c \cup B, \tag{24}$$

$$0 = \int_B M^I(s,x)w(s)\mathrm{d}B(s) - \int_B L^I(s,x)\frac{\partial w(s)}{\partial n_s}\mathrm{d}B(s), \quad x \in D^c \cup B, \tag{25}$$

once the kernel is expressed in terms of an appropriate degenerate form (the superscripts of "E" and "I" denote exterior and interior cases, respectively). It is found that the collocation point is categorized to three regions, domain (Eqs. (12)–(13)), boundary (Eqs. (18)–(19)) and complementary domain (Eqs. (20)–(21)) in the conventional formulation. After using the degenerate kernel for the null-field BIEM, Eqs. (22)–(23) and Eqs. (24)–(25) can include the boundary point. In the real implementation, we obtain the linear algebraic equation by using the limiting process of $x \to B^+$ or B^- in companion with the corresponding degenerate kernel. For the boundary densities in Fig. 2c, we introduce the degenerate kernel to describe the potentials. More details are shown in the next section.

2.3 Expansions of fundamental solutions and boundary densities

To fully employ the property of circular geometry, the mathematical tools, degenerate kernel (so-called separable kernel) and Fourier series, are utilized for an analytical study.

2.3.1 Degenerate (separable) kernel

Based on the separable property, the kernel function $U(s, \mathrm{x})$ can be expanded into degenerate form by separating the source point and field point in the polar coordinate

$$U(s,x) = \begin{cases} U^I(R,\theta;\rho,\phi) = \ln R - \sum_{m=1}^{\infty} \frac{1}{m}\left(\frac{\rho}{R}\right)^m \cos m(\theta-\phi), & R \geq \rho, \\ U^E(R,\theta;\rho,\phi) = \ln \rho - \sum_{m=1}^{\infty} \frac{1}{m}\left(\frac{R}{\rho}\right)^m \cos m(\theta-\phi), & R < \rho, \end{cases} \tag{26}$$

where the superscripts "I" and "E" denote the interior ($R \geq \rho$) and exterior ($R < \rho$) cases, respectively. In order to ensure the log singularity and the series convergence, the leading term and the denominator in the above expansion are dominated by the larger argument. After taking the derivative operators in Eqs. (15)–(17), the $T(s,x)$, $L(s,x)$ and $M(s,x)$ kernels can be easily derived and the detailed representation can be found in [4]. It is noted that the null-field point in Eq. (24) or the domain point in Eq. (22) can be exactly located on the real boundary when the appropriate degenerate kernels are employed. Our formulation for Eqs. (22)–(25) can be used for the point x on the real boundary free of singular integrals, while the conventional BEM needs to deal with singularities since a closed-form kernel is used. For a rigorous definition, the degenerate kernel is a finite-rank expansion of the closed-form fundamental solution.

2.3.2 Fourier series expansion for boundary density

The unknown boundary densities are represented by using the Fourier series as shown below:

$$w(s_k) = a_0^k + \sum_{n=1}^{\infty} (a_n^k \cos n\theta_k + b_n^k \sin n\theta_k), \quad s_k \in B_k, \quad k = 1, 2, \ldots, H, \tag{27}$$

$$\frac{\partial w(s_k)}{\partial n_s} = p_0^k + \sum_{n=1}^{\infty} (p_n^k \cos n\theta_k + q_n^k \sin n\theta_k), \quad s_k \in B_k, \quad k = 1, 2, \ldots, H, \tag{28}$$

where a_n^k, b_n^k, p_n^k and $q_n^k (n = 1, 2, \ldots)$ are the Fourier coefficients, θ_k is the polar angle measured related to the x-direction and H is the number of circular boundary. In the real computation, the finite number of terms M for boundary density is adopted.

2.4 Adaptive observer system

To analytically determine the boundary contour integrations of a problem containing multiple circular boundaries, the degenerate kernel for translating the solution of a screw dislocation may be required. In order to fully employ the property of degenerate kernels for circular boundaries, an adaptive observer system is addressed as shown in Fig. 6. Figure 6 shows the boundary contour integration for the circular boundaries. For the boundary integrals, the origin of the observer system can be adaptively located on the center of the corresponding circular boundary under integration. The dummy variable in the circular boundary integration is the angle, θ, instead of the radial coordinate R. By using the adaptive observer system, all the integrals can be easily calculated for multiple holes.

2.5 Linear algebraic equation

In order to calculate the Fourier coefficients, $N(N = 2M + 1)$ boundary nodes for each circular boundary are located uniformly on each circular boundary. From Eqs. (22) and (23), we have

$$0 = \sum_{i=1}^{H} \int_{B_i} T(s,x) w(s) \mathrm{d}B(s) - \sum_{i=1}^{H} \int_{B_i} U(s,x) \frac{\partial w(s)}{\partial n_s} \mathrm{d}B(s), \quad x \in D^c \cup B, \tag{29}$$

$$0 = \sum_{i=1}^{H} \int_{B_i} M(s,x) w(s) \mathrm{d}B(s) - \sum_{i=1}^{H} \int_{B_i} L(s,x) \frac{\partial w(s)}{\partial n_s} \mathrm{d}B(s), \quad x \in D^c \cup B. \tag{30}$$

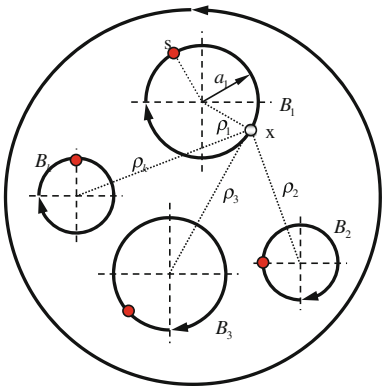

Fig. 6 Sketch of the null-field integral equation in conjunction with the adaptive observer system

It is noted that the integration path is clockwise. For the integral of the circular boundary B_i, the kernels ($U(s,x)$, $T(s,x)$, $L(s,x)$ and $M(s,x)$) are expressed by using the degenerate kernel and setting the origin at the center of B_i. The boundary densities $\left(w(s) \text{ and } \frac{\partial w(s)}{\partial n_s}\right)$ are substituted by using the degenerate kernel and Fourier series. From Eq. (29), a linear algebraic system yields

$$[\mathbf{U}]\left\{\frac{\partial \mathbf{w}}{\partial \mathbf{n}}\right\} = [\mathbf{T}]\{\mathbf{w}\}, \tag{31}$$

where $[\mathbf{U}]$ and $[\mathbf{T}]$ are the influence matrices with a dimension of $H \times (2M+1)$ by $H \times (2M+1)$, $\{\mathbf{w}\}$ and $\left\{\frac{\partial \mathbf{w}}{\partial \mathbf{n}}\right\}$ denote the column vectors of Fourier coefficients with a dimension of $H \times (2M+1)$ by 1 for $\mathbf{w}$ and $\frac{\partial \mathbf{w}}{\partial \mathbf{n}}$, respectively. All the unknown coefficients can be solved from the linear algebraic equation in Eq. (31). Then, the unknown boundary data can be determined, and the potential is obtained by substituting the boundary data into Eq. (22). Based on the null-field integral equation approach, successful applications to Laplace [4], Helmholtz [8], biharmonic [7] and biHelmholtz [15] problems were presented.

2.6 Matching of interface conditions and solution procedures

After decomposing the inclusion problems, we employ the null-field integral equation approach to handle the exterior BVP in Fig. 2b and multiple inclusions problem as shown in Fig. 2d. In our approach, the null-field points are exactly collocated on the real boundary and the linear algebraic system is obtained easily. For the exterior problem in Fig. 2d, the null-field integral equation yields

$$[\mathbf{U}^M]\left\{\frac{\partial \mathbf{w}^M}{\partial \mathbf{n}} - \frac{\partial \mathbf{w}^{sd}}{\partial \mathbf{n}}\right\} = [\mathbf{T}^M]\left\{\mathbf{w}^M - \mathbf{w}^{sd}\right\}, \tag{32}$$

where the superscripts "M" and "sd" denote the matrix and screw dislocation, respectively. For more detail on the null-field integral equation, readers can consult with [4]. For the interior problem of each inclusion in Fig. 2b, we have

$$[\mathbf{U}^I]\left\{\frac{\partial \mathbf{w}^I}{\partial \mathbf{n}}\right\} = [\mathbf{T}^I]\left\{\mathbf{w}^I\right\}, \tag{33}$$

where the superscript "I" denotes the inclusion. $[\mathbf{U}^M]$, $[\mathbf{T}^M]$, $[\mathbf{U}^I]$ and $[\mathbf{T}^I]$ are the influence matrices and are obtained from the degenerate kernels. The boundary data of $\left\{\frac{\partial \mathbf{w}^M}{\partial \mathbf{n}}\right\}$, $\left\{\frac{\partial \mathbf{w}^I}{\partial \mathbf{n}}\right\}$, $\left\{\mathbf{w}^M\right\}$ and $\left\{\mathbf{w}^I\right\}$ are the vectors of Fourier coefficients. According to the continuity of displacement and the equilibrium of traction along the ideal interface, we have the constraints

$$\left\{\mathbf{w}^M\right\} = \left\{\mathbf{w}^I\right\}, \quad \text{on } B, \tag{34}$$

$$[\boldsymbol{\mu}_M]\left\{\frac{\partial \mathbf{w}^M}{\partial \mathbf{n}}\right\} = -[\boldsymbol{\mu}_I]\left\{\frac{\partial \mathbf{w}^I}{\partial \mathbf{n}}\right\}, \quad \text{on } B, \tag{35}$$

where $[\boldsymbol{\mu}_I]$ and $[\boldsymbol{\mu}_M]$ are shown as follows:

$$[\boldsymbol{\mu}_I] = \begin{bmatrix} \mu_I & 0 & \dots & 0 \\ 0 & \mu_I & \dots & 0 \\ \vdots & \vdots & \ddots & \vdots \\ 0 & 0 & \dots & \mu_I \end{bmatrix}, \quad [\boldsymbol{\mu}_M] = \begin{bmatrix} \mu_M & 0 & \dots & 0 \\ 0 & \mu_M & \dots & 0 \\ \vdots & \vdots & \ddots & \vdots \\ 0 & 0 & \dots & \mu_M \end{bmatrix}, \tag{36}$$

in which μ_I and μ_M denote the shear modulus of the matrix and the inclusion, respectively. By assembling matrices in Eqs. (32)–(35), a global algebraic system can be obtained as follows:

$$\begin{bmatrix} T^M & -U^M & 0 & 0 \\ 0 & 0 & T^I & -U^I \\ I & 0 & -I & 0 \\ 0 & \mu_M & 0 & \mu_I \end{bmatrix} \begin{Bmatrix} w^M \\ \frac{\partial w^M}{\partial n} \\ w^I \\ \frac{\partial w^I}{\partial n} \end{Bmatrix} = \begin{Bmatrix} c \\ 0 \\ 0 \\ 0 \end{Bmatrix}, \tag{37}$$

where the matrix $[I]$ is an identity matrix and $\{c\}$ is the forcing term due to the screw dislocation, which is represented as

$$\{c\} = [T^M] \left\{ w^{sd} \right\} - [U^M] \left\{ \frac{\partial w^{sd}}{\partial n} \right\}. \tag{38}$$

By translating the screw dislocation to the origin of the circular hole, the boundary distribution of w^{sd} and $\frac{\partial w^{sd}}{\partial n}$ due to the screw dislocation are expressed as

$$w^{sd} = \begin{cases} \theta + \sum_{m=1}^{\infty} \frac{1}{m} \left(\frac{a_i}{R} \right)^m \sin m(\theta - \phi), & a_i < R, \\ \phi - \pi - \sum_{m=1}^{\infty} \frac{1}{m} \left(\frac{R}{a_i} \right)^m \sin m(\theta - \phi), & a_i > R, \end{cases} \tag{39}$$

$$\frac{\partial w^{sd}}{\partial n} = \begin{cases} \sum_{m=1}^{\infty} \frac{a_i^{m-1}}{R^m} \sin m(\theta - \phi), & a_i < R, \\ \sum_{m=1}^{\infty} \frac{R^m}{a_i^{m+1}} \sin m(\theta - \phi), & a_i > R, \end{cases} \tag{40}$$

where R and θ denote the distance and polar angle, respectively, between the screw dislocation and the origin as shown in Fig. 3 and a_i denotes the radius of the i-th circle. The flowchart of the present approach is shown in Fig. 7.

3 Illustrative examples and discussions

Case 1 An infinite plane with a rigid inclusion subject to the Dirichlet boundary condition (an analytical solution)

Figure 8a shows the geometry of a rigid inclusion in an infinite plane with the screw dislocation subject to the Dirichlet boundary condition of $w = 0$. The screw dislocation is located at $(x, y) = (1.75, 0)$. The center of the rigid inclusion is set at $(0, 0)$ and the radius a is 1.5 m. An analytical solution was derived by Smith [18] as shown below:

$$\begin{aligned} F(z) &= \frac{\mu_E b}{2\pi i} \ln(z - z_0) + \frac{\mu_E b}{2\pi i} \ln \left(\frac{a^2}{z} - \bar{z}_0 \right), \\ w(x, y) &= \frac{1}{\mu_E} Re[F(z)], \end{aligned} \tag{41}$$

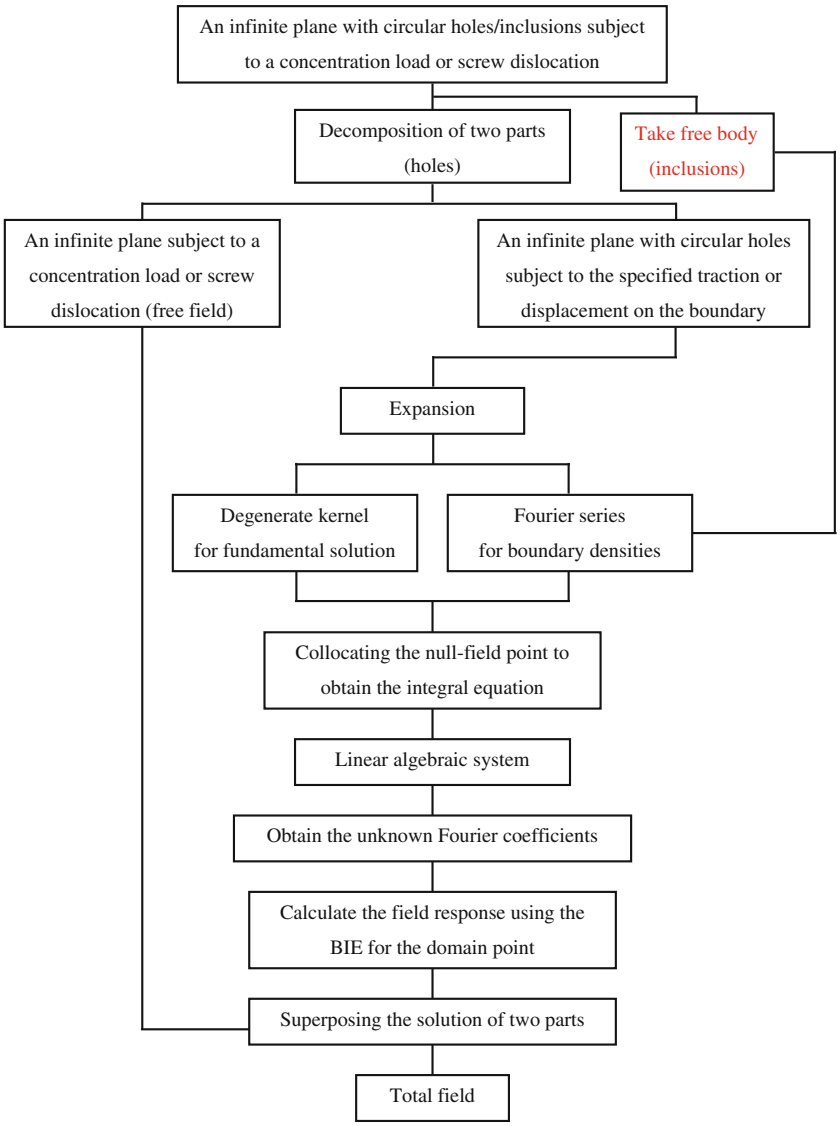

Fig. 7 Flowchart of the present method

where $F(z)$ and μ_E denote the complex-variable function and shear modulus, respectively, $\bar{z}_0$ denotes the conjugate of the position vector of the screw dislocation, b denotes the Burgers' vector, and $Re[\cdot]$ denotes the real part. By using the present formulation, the analytical solution is obtained as shown below:

$$w(\rho,\phi)=\begin{cases}\left(1-\dfrac{\ln\rho}{\ln a}\right)\dfrac{b\theta}{2\pi}+\displaystyle\sum_{m=1}^{\infty}\frac{b}{2\pi m}\left[\left(\frac{\rho}{R}\right)^m-\left(\frac{a^2}{\rho R}\right)^m\right]\sin m(\theta-\phi), & R\geq\rho,\\ \dfrac{b\phi}{2\pi}-\dfrac{b}{2}-\dfrac{\ln\rho}{\ln a}\dfrac{b\theta}{2\pi}-\displaystyle\sum_{m=1}^{\infty}\frac{b}{2\pi m}\left[\left(\frac{R}{\rho}\right)^m+\left(\frac{a^2}{\rho R}\right)^m\right]\sin m(\theta-\phi), & R<\rho,\end{cases}\tag{42}$$

Figure 8b and c shows the potential distribution by using the Smith method [18] and the present method, respectively. It is found that the result of the present approach compares well with those of using the Simth's method. Based on the degenerate kernel, it is easier to find the image location of (a^2/R) with the negative strength. A similar work can be found for the image location of source case [5].

Case 2 An infinite plane with a hole subject to the Neumann boundary condition (an analytical solution).

Figure 9a shows the geometry of a single hole in the infinite plane with the screw dislocation. The screw dislocation is located at $(x, y) = (1.75, 0)$. The center of the hole is set at $(0, 0)$, and the radius a is 1.5 m.

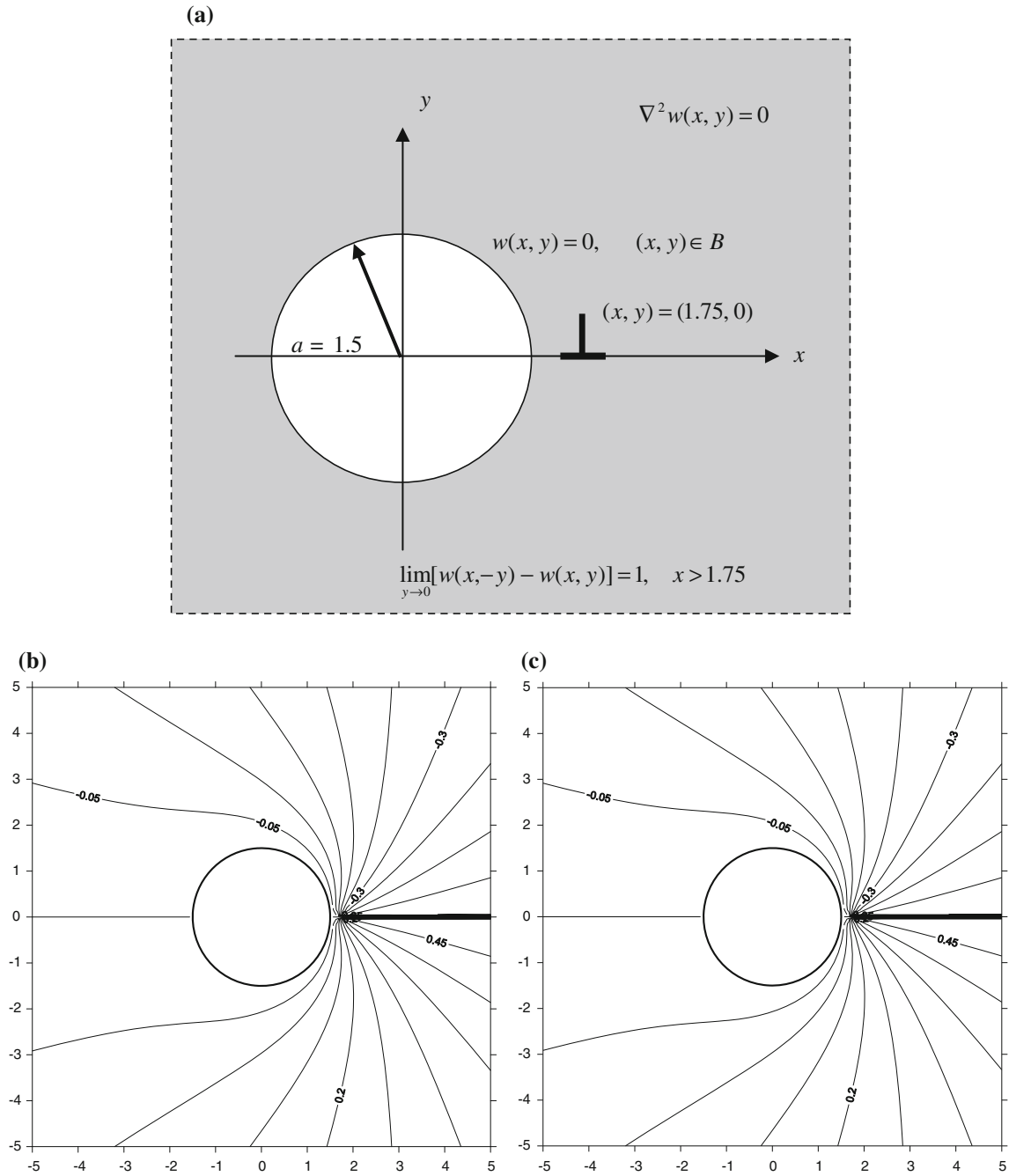

Fig. 8 **a** An infinite plane with a circular rigid inclusion (Dirichlet boundary condition) subject to the screw dislocation; **b** Potential contour by using the Smith method [15]; **c** Potential contour by using the present method ($M = 50$)

The analytical solution proposed by Smith is found in [18] as

$$F(z) = \frac{\mu_E b}{2\pi i} \ln(z - z_0) - \frac{\mu_E b}{2\pi i} \ln\left(\frac{a^2}{z} - \bar{z}_0\right),$$
$$w(x, y) = \frac{1}{\mu_E} Re[F(z)], \tag{43}$$

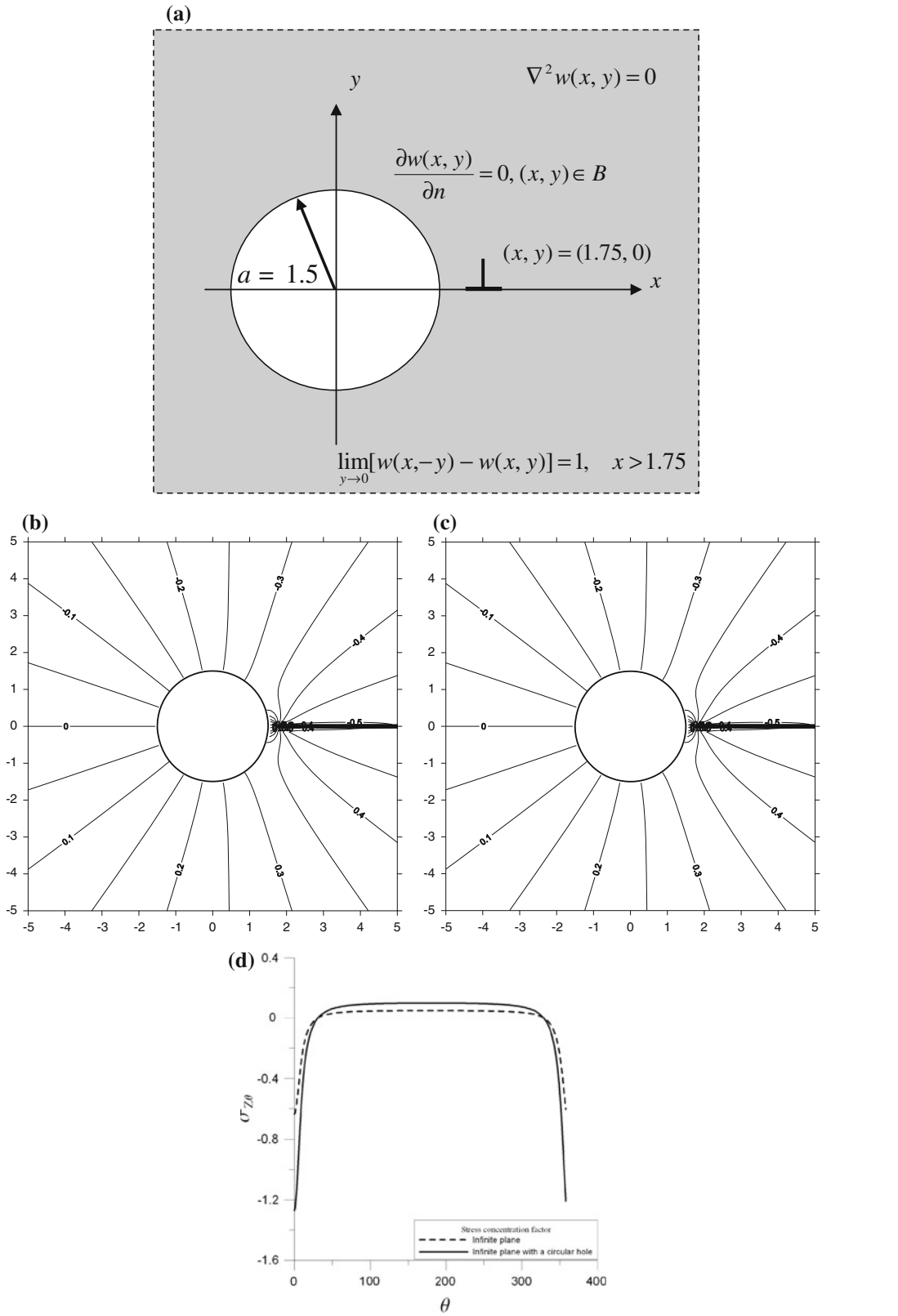

Fig. 9 **a** An infinite plane with a circular hole (Neumann boundary condition) subject to the screw dislocation; **b** Potential contour by using the Smith method [15]; **c** Potential contour by using the present method ($M = 50$); **d** Stress distribution along the circular hole

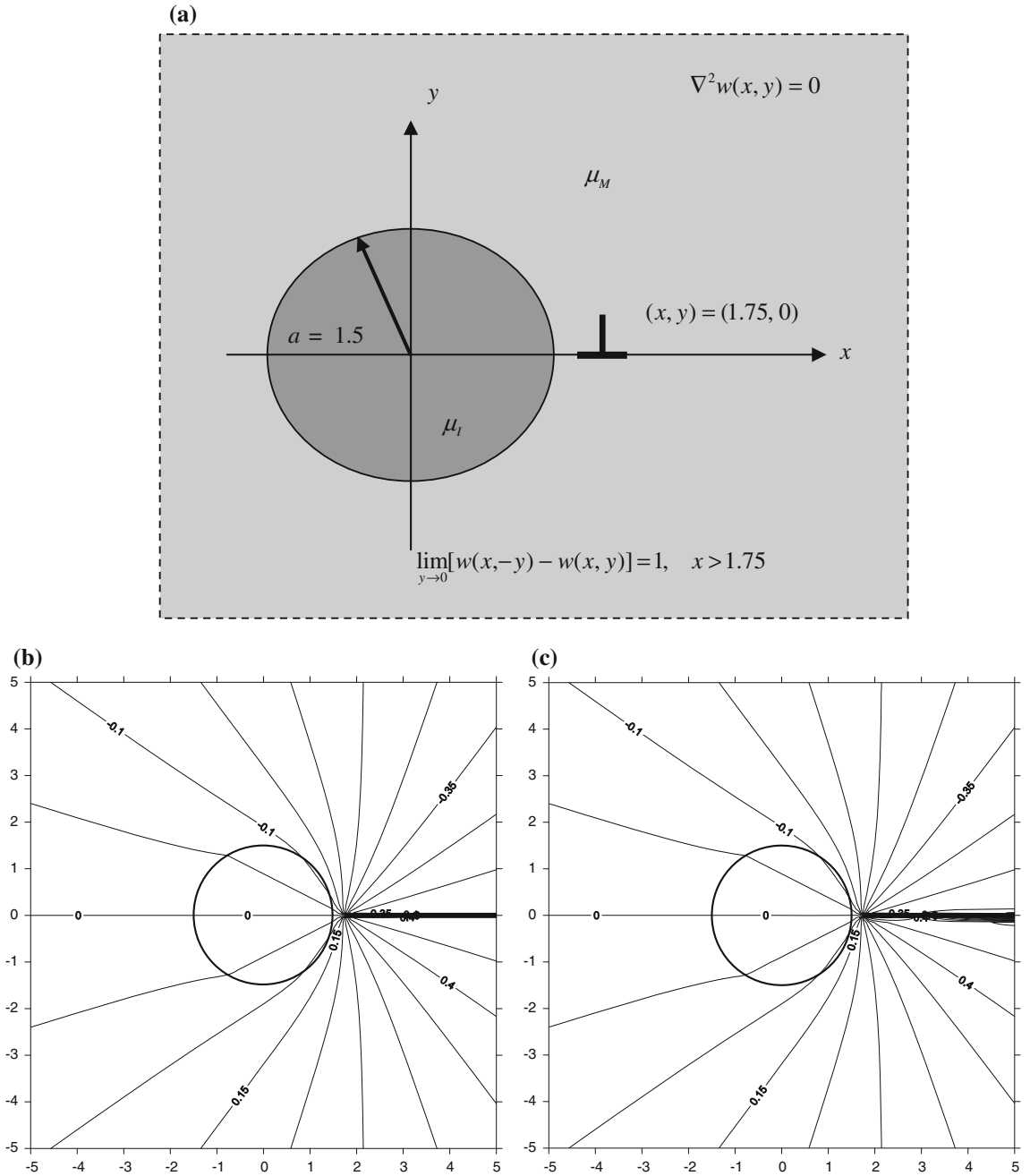

Fig. 10 **a** A circular inclusion embedded in the matrix subject to the screw dislocation; **b** Potential contour by using the Smith method (1968); **c** Potential contour by using the present method ($M = 50$)

By using the present formulation, the analytical solution is derived as shown below:

$$w(\rho,\phi)=\begin{cases}\dfrac{b\theta}{2\pi}+\displaystyle\sum_{m=1}^{\infty}\frac{b}{2\pi m}\left[\left(\frac{\rho}{R}\right)^m+\left(\frac{a^2}{\rho R}\right)^m\right]\sin m(\theta-\phi), & R\geq\rho,\\ \dfrac{b\phi}{2\pi}-\dfrac{b}{\pi}-\displaystyle\sum_{m=1}^{\infty}\frac{b}{2\pi m}\left[\left(\frac{R}{\rho}\right)^m-\left(\frac{a^2}{\rho R}\right)^m\right]\sin m(\theta-\phi), & R<\rho,\end{cases} \tag{44}$$

Figure 9b and c shows the potential distribution by using the Smith method [18] and the present method, respectively. Good agreement is seen. By expanding the Smith's solution through the degenerate kernel,

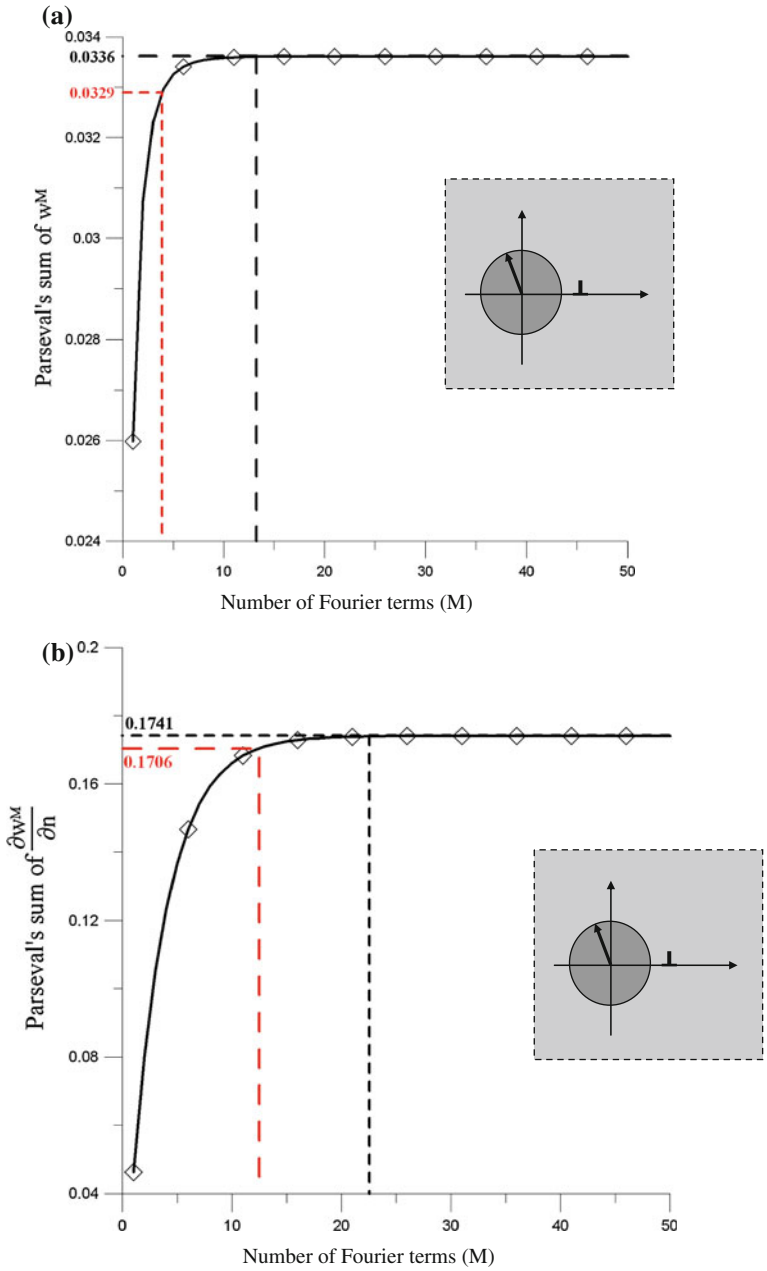

Fig. 11 **a** Parseval's sum for w^M with $a = 1.5$ and $(x, y) = (1.75,\ 0)$; **b** Parseval's sum for $\frac{\partial w^M}{\partial n}$ with $a = 1.5$ and $(x, y) = (1.75,\ 0)$

we have

$$w_s(\rho,\phi) = \begin{cases} \dfrac{b\theta}{\pi} + \displaystyle\sum_{m=1}^{\infty} \frac{b}{2\pi m}\left[\left(\frac{\rho}{R}\right)^m + \left(\frac{a^2}{\rho R}\right)^m\right]\sin m(\theta-\phi), & R \geq \rho, \\ \dfrac{b\phi}{2\pi} + \dfrac{b\theta}{2\pi} - \dfrac{b}{2} - \displaystyle\sum_{m=1}^{\infty} \frac{b}{2\pi m}\left[\left(\frac{R}{\rho}\right)^m - \left(\frac{a^2}{\rho R}\right)^m\right]\sin m(\theta-\phi), & R < \rho, \end{cases} \tag{45}$$

where the subscript "s" denotes the Smith's solution. After comparing with the two solutions, there is a little difference between the present approach and Smith's work as θ is not equal to zero. The θ term can be viewed as a rigid body solution due to the Neumann problem. The stress distribution along the circular hole is shown

in Fig. 9d. The stress on the artificial boundary of an infinite plane subject to the dislocation yields

$$\sigma_{z\theta} = -\frac{1}{2\pi\rho}\sum_{m=1}^{\infty}\left(\frac{\rho}{R}\right)^m \cos(m(\theta-\phi)). \tag{46}$$

For an infinite plane with a circular hole, the stress on the circular boundary is obtained as follows:

$$\sigma_{z\theta} = -\frac{1}{2\pi\rho}\sum_{m=1}^{\infty}\left(\frac{\rho^m}{R^m} + \left(\frac{a^2}{\rho R}\right)^m\right)\cos(m(\theta-\phi)). \tag{47}$$

It is worthy of noting that the stress concentration factor (SCF) on the circular boundary ($\rho = a$) is two where the SCF is the ratio of stress in an infinite plane with a hole over free space subject to the screw dislocation.

Case 3 An infinite plane with a circular inclusion (an analytical solution)

Figure 10a shows the geometry of a single inclusion in the infinite plane with the screw dislocation. The screw dislocation is located at $(x, y) = (1.75, 0)$. The center of the hole is set at $(0, 0)$ and the radius a is 1.5 m. The analytical solution proposed by Smith was found in [18] as

$$\begin{aligned} F_I(z) &= \frac{(1+k)\mu_E b}{2\pi i}\ln(z-z_0),\\ F_E(z) &= \frac{\mu_E b}{2\pi i}\ln(z-z_0) + \frac{k\mu_E b}{2\pi i}\ln\left(\frac{a^2}{z} - \bar{z}_0\right),\\ w_I(x,y) &= \frac{1}{\mu_I}Re[F_I(z)],\\ w_E(x,y) &= \frac{1}{\mu_E}Re[F_E(z)], \end{aligned} \tag{48}$$

where the subscripts "I" and "E" denote the inside and outside of the inclusion, respectively, μ_I and μ_E denote the shear modulus for the inclusion and matrix, respectively, and $k = (\mu_I - \mu_E)/(\mu_I + \mu_E)$. By using the present formulation, the analytical solution is shown below:

$$w(\rho,\phi) = \begin{cases} \frac{b\theta}{2\pi} + \sum_{m=1}^{\infty}\frac{b}{2\pi m}\left[\left(\frac{\rho}{R}\right)^m + \frac{\mu_M-\mu_I}{\mu_M+\mu_I}\left(\frac{a^2}{\rho R}\right)^m\right]\sin m(\theta-\phi), & \rho \geq a \text{ and } \rho \leq R,\\ \frac{b(\phi-\pi)}{2\pi} - \sum_{m=1}^{\infty}\frac{b}{2\pi m}\left[\left(\frac{R}{\rho}\right)^m - \frac{\mu_M-\mu_I}{\mu_M+\mu_I}\left(\frac{a^2}{\rho R}\right)^m\right]\sin m(\theta-\phi), & \rho \geq a \text{ and } \rho > R,\\ \frac{b\theta}{2\pi} + \sum_{m=1}^{\infty}\frac{b}{\pi m}\left(\frac{\rho}{R}\right)^m\frac{\mu_M}{\mu_M+\mu_I}\sin m(\theta-\phi), & \rho < a, \end{cases} \tag{49}$$

where μ_M and μ_I denote the shear moduli of the matrix and inclusion, respectively. Figure 10b and c shows the potential distribution by using the Smith method [18] and the present method, respectively. The result of Case 2 can be obtained by using the limiting process ($\mu_I \to 0$). Furthermore, Parseval's theorem is adopted to test the convergence for different number of terms (M) for the Fourier series since the boundary densities are continuous on $[0,\ 2\pi]$. Parseval's theorem is defined as shown below:

$$\int f^2(\theta)d\theta \approx 2\pi a_0^2 + \pi\sum_{n=1}^{M}\left(a_n^2 + b_n^2\right), \tag{50}$$

where

$$f(\theta) = a_0 + \sum_{n=1}^{M}(a_n\cos n\theta + b_n\sin n\theta). \tag{51}$$

According to Eq. (49), the Parseval sum versus various number of terms (M) of the Fourier series of boundary densities on each circular boundary in the screw dislocation is plotted in Fig. 11a and b. The value marked by dashed lines is the error of 2%. In the tolerance of this error, only five and fifteen truncated terms are required for displacement and stress, respectively.

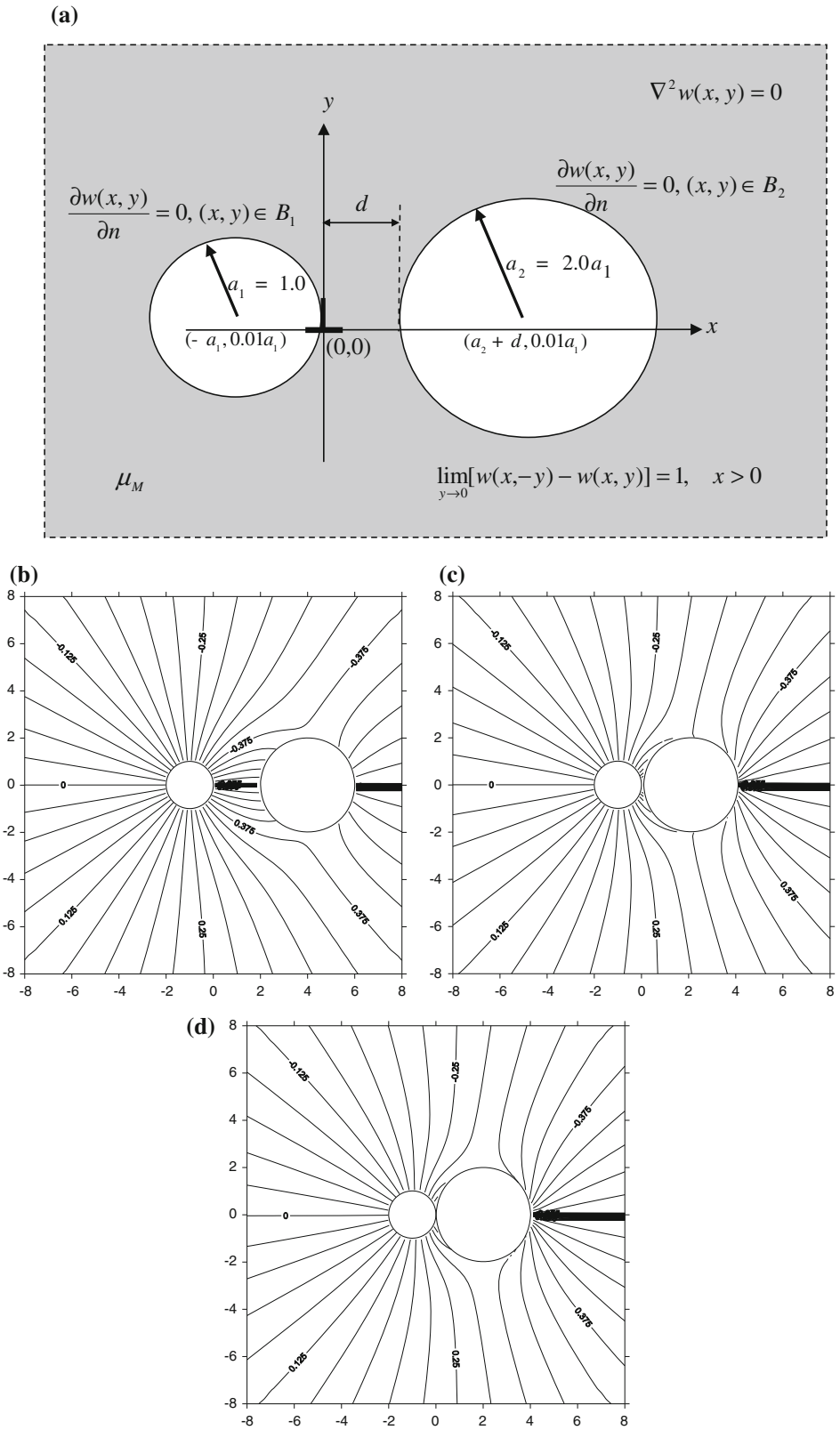

Fig. 12 **a** An infinite plane with two circular holes (Neumann boundary condition) subject to the screw dislocation; **b** The displacement contour for the two circular holes problem ($d = 2.0a_1$, $M = 50$); **c** The displacement contour for the two circular holes problem ($d = 0.1a_1$, $M = 50$); **d** The displacement contour for the two circular holes problem ($d = 0.01a_1$, $M = 50$)

Case 4 An infinite plane with two circular holes (semi-analytical solution).

Following the success of the single-hole case to compare well with the Smith's result, we extend to two circular holes as shown in Fig. 12a to show the generality of our approach. The screw dislocation is located at $(x, y) = (0, 0)$. The center of the two holes are set at $(-a_1, 0.01a_1)$ and $(d + a_2, 0.01a_1)$. The radii a_1 and a_2 are 1.0 m and $2.0a_1$, respectively. Three cases of $d = 2.0a_1, 0.1a_1$ and $0.01a_1$ are demonstrated to show the validity of the present method. The contour of displacement for the two circular holes problem is shown in Fig. 12b–d. In this case, the analytical solution cannot be derived. A numerical solution instead of an analytical one is obtained in this case. Fifty terms of the Fourier series are used, and 101 collocation points are distributed on each circle. Since the error comes from the number of truncation terms, the proposed approach can be called a semi-analytical approach.

4 Conclusions

For the screw dislocation problem with circular holes and/or inclusions, we have proposed a logical approach to construct the screw dislocation solution by using the degenerate kernel and superposition technique. The angle-type fundamental solution for the screw dislocation was first derived in terms of degenerate kernel in this paper. Several examples including an infinite plane with a circular boundary subject to the Dirichlet or Neumann boundary condition and a circular inclusion imbedded in an infinite plane were demonstrated to check the validity of the present formulation. A case of two holes was also addressed. Neither complex-variable technique nor senses of principal values were required. Good agreements were made after comparing with the previous results. Based on the developed concept, the extension to three dimension is now under investigation.

Acknowledgments Financial support from the National Science Council under the Grant No. NSC-98-2221-E-019-017-Mr3 for Taiwan Ocean University is gratefully acknowledged.

References

1. Ang, W.T., Kang, I.: A complex variable boundary element method for elliptic partial differential equations in a multiply connected region. Int. J. Comput. Math. **75**, 515–525 (2000)
2. Atkinson, K.E.: The Numerical Solution of Integral Equations of the Second Kind. Cambridge University Press, New York (1997)
3. Chen, Y.Z., Lin, X.Y.: Solutions of the interior and exterior boundary value problems in plane elasticity by using dislocation distribution layer. Int. J. Solids Struct. **47**, 355–364 (2010)
4. Chen, J.T., Shen, W.C., Wu, A.C.: Null-field integral equations for stress field around circular holes under anti-plane shear. Eng. Anal. Bound. Elem. **30**, 205–217 (2005)
5. Chen, J.T., Wu, C.S.: Alternative derivations for the Poisson integral formula. Int. J. Math. Educ. Sci. Technol. **37**, 165–185 (2006)
6. Chen, J.T., Shen, W.C.: Degenerate scale for multiply connected Laplace problems. Mech. Res. Commun. **34**, 69–77 (2007)
7. Chen, J.T., Hsiao, C.C., Leu, S.Y.: Null-field approach for Laplace problems with circular boundaries using degenerate kernels. ASME J. Appl. Mech. **73**, 679–693 (2007)
8. Chen, J.T., Chen, C.T., Chen, P.Y., Chen, I.L.: A semi-analytical approach for radiation and scattering problems with circular boundaries. Comput. Methods Appl. Mech. Eng. **196**, 2751–2764 (2008)
9. Dundurs, J.: Elastic interaction of dislocations with inhomogeneities. In: Mura, T. (ed.) Mathematical Theory of Dislocations, pp. 70–115. American Society of Mechanical Engineers, New York (1969)
10. Fan, H., Wang, G.F.: Screw dislocation interacting with imperfect interface. Mech. Mater. **35**, 943–953 (2003)
11. Fang, Q.H., Liu, Y.W.: Size-dependent elastic interaction of a screw dislocation with a circular nano-inhomogeneity incorporating interface stress. Scr. Mater. **55**, 99–102 (2006)
12. Golberg, M.A.: Solution Methods for Integral Equations: theory and Applications. Plenum Press, New York (1979)
13. Honein, E., Honein, T., Herrmann, G.: On two circular inclusions in harmonic problems. Q. Appl. Math. **50**(3), 479–499 (1992)
14. Jin, B., Fang, Q.H.: Piezoelectric screw dislocations interacting with a circular inclusion with imperfect interface. Arch. Appl. Mech. **78**, 105–116 (2008)
15. Lee, W.M., Chen, J.T.: Null-field integral equation approach for free vibration analysis of circular plates with multiple circular holes. Comput. Mech. **42**, 733–747 (2008)
16. Porter, D., Stirling, D.S.G.: Integral Equations: a Practical Treatment, from Spectral Theory to Applications. Cambridge University Press, New York (1990)
17. Sendeckyj, G.P.: Screw dislocations near circular inclusions. Phys. Stat. Sol. **3**, 529–535 (1970)
18. Smith, E.: The interaction between dislocations and inhomogeneities-I. Int. J. Eng. Sci. **6**, 129–143 (1968)
19. Sudak, L.J.: On the interaction between a dislocation and a circular inhomogeneity with imperfect interface in antiplane shear. Mech. Res. Commun. **30**, 53–59 (2002)